

# Deep Representation Learning for Domain Adaptation of Semantic Image Segmentation

Assia Benbihi<sup>1</sup>  
abenbihi@georgiatech-metz.fr

Matthieu Geist<sup>2</sup>  
matthieu.geist@univ-lorraine.fr

Cedric Pradalier<sup>1</sup>  
cedric.pradalier@georgiatech-metz.fr

<sup>1</sup> UMI 2958 GT-CNRS – GeorgiaTech  
Lorraine  
Metz, France

<sup>2</sup> Université de Lorraine  
CNRS LIEC UNR 7360,  
Metz, France

---

## Abstract

Deep Convolutional Neural Networks have pushed the state-of-the-art for semantic segmentation provided that a large amount of images together with pixel-wise annotations is available. Data collection is expensive and a solution to alleviate it is to use transfer learning. This reduces the amount of annotated data required for the network training but it does not get rid of this heavy processing step. We propose a method of transfer learning without annotations on the target task for datasets with redundant content and distinct pixel distributions. Our method takes advantage of the approximate content alignment of the images between two datasets when the approximation error prevents the reuse of annotation from one dataset to another. Given the annotations for only one dataset, we train a first network in a supervised manner. This network autonomously learns to generate deep data representations relevant to the semantic segmentation. Then the images in the new dataset, we train a new network to generate a deep data representation that matches the one from the first network on the previous dataset. The training consists in a regression between feature maps and does not require any annotations on the new dataset. We show that this method reaches performances similar to a classic transfer learning on the PASCAL VOC dataset with synthetic transformations.

## 1 Introduction

Many applications such as environment monitoring or medical image processing rely of semantic segmentation of datasets with redundant content. Deep Convolutional Neural Networks (DCNN) reach state-of-the-art performance on segmentation on such datasets but require a large amount of data together with pixel-wise annotations. These types of applications share a common feature which is that the segmentation dataset gets larger with time and the data distribution may change. This prevents a network trained on a dataset at time  $t$  to generalize a latter time. Each time the pixel distribution deviates too much from the past, the network needs to be fine-tuned or retrained from scratch. In both cases, one needs to provide new pixel-wise annotations as the dataset changes. To avoid the burden of re-annotation, we propose a method to transfer the learning from a network trained at time  $t$  to the dataset at time  $t+1$  without annotations on the new dataset. To do so, we transfer the

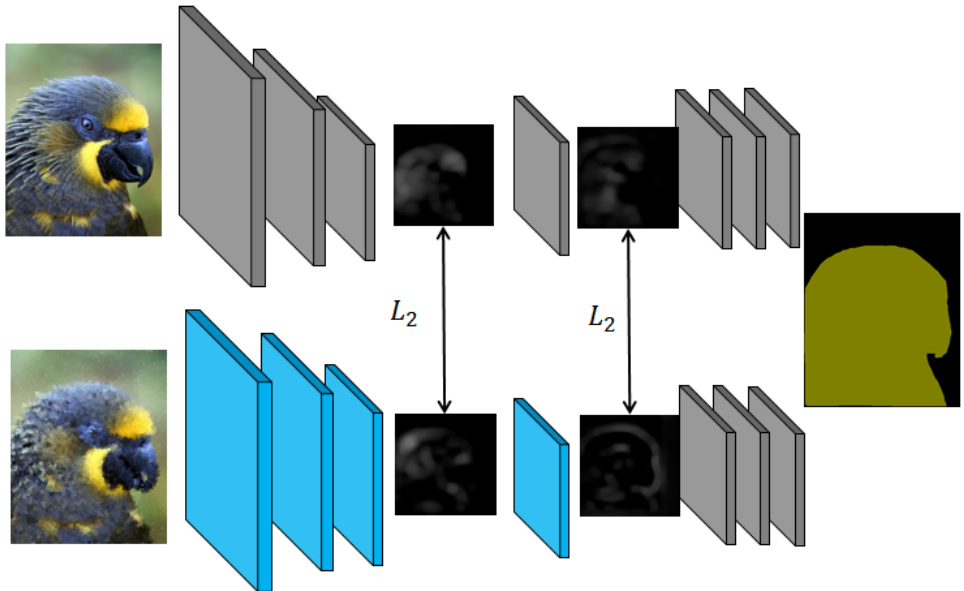


Figure 1: Top: The trained and frozen (gray) network provides ground truth deep representations. Down: The trainable layers (blue) must learn the deep representations.

deep representations learned by the network at time  $t$  instead of transferring the whole segmentation learning. This method has been studied in [14] in the Unsupervised and Transfer Learning Challenge for classification. One of the limitation in this work was the lack of instances pairs with the same semantic content. In the applications we address, such pairs arise naturally which solves this issue.

For example, environment monitoring surveys the same area across time. This generates several datasets with approximately aligned images across surveys. One could provide annotations for a small part of the dataset to train the network and then generalize it to the future. However, the image distribution may change across time which prevent a good generalization. In [15], a DCNN is used to segment land categories on aerial images over a period from 1955 to 2015. The 2015 dataset is made of RGB digital images whereas the 1955 data is made of black and white analog images that have been digitized. A network trained on the 2015 data can not generalize on the 1955 because the images do not have the same color domain nor the same resolution or grain. Also, even though the surveys cover the same area, the images are not perfectly aligned due to small changes in land use, which prevent the use of 2015 annotations to train a network on the 1955 data. What stays approximately invariant for one image across surveys is the high-level semantic content. DCNN have the property to autonomously build high-level data representation in the feature maps during supervised training. Our method proposes to train a network  $H_1$  only on one of the dataset  $D_1$  with pixel-wise supervision. Then a second network  $H_2$  is trained to generate deep representations for another dataset  $D_2$  so as to match the deep representation of  $H_1$  on  $D_1$ .

We apply this method to synthetic transformations on the PASCAL VOC 12. We use synthetic data to gather ideal baselines that require to have pixel-wise annotations on all datasets. We show that our transfer learning method reach the same performance as clas-

sic transfer learning and classic training. The next section describes the state-of-the-art in transfer learning for DCNN. Section 3 and 4 presents our method and results.

## 2 Related work

Transfer learning [14] is relevant for DCNN because convolution filters can be transferred as-is from one network to another and it solves a main issue which is collecting enough data for the network training to converge. There are two main categories of transfer learning that the literature addresses: inductive transfer learning and transductive transfer learning. Inductive transfer learning consists in transferring the weights of a network trained on a different task but on the same dataset distribution. This is relevant because the early layers of a DCNN capture low-level image features such as colours or edges [19] which are agnostic to the task. Given one dataset, they can be reused as-is as a foundation on which to build high-level features that will be specialised to the task at hands in deeper layers. For example, [10] extend a classification network with fully connected layer to a fully convolutional layer for semantic segmentation. They keep the first layers of the network which build high level representations such as object contours and replace the fully connected layers with convolutional layers. These last layers are trained from scratch and compute the segmentation labels from the representation built by the lower layers. State-of-the art segmentation networks such as DeepLab [8] and SegNet [11] also use this approach.

Transductive transfer on the other hand consists in transferring the weights of a network trained to do the same task but on an other dataset. This is a classic method to decrease the amount of data needed to train a network. For example, [9] propose to train a network to compute the flow between two images with supervised learning. However, it is extremely complex to generate real data with ground truth flow. So the authors created the Flying Chair synthetic dataset to train the network. Then, they trained this network on a reduced set of the target dataset. Pre-training on synthetic data is also relevant for urban scenes segmentation as demonstrated in [16]. Our method is similar in that we initialise  $H_2$  with the weights of the supervised training of  $H_1$ . However, we do not train  $H_2$  on the target task which is semantic segmentation. We train  $H_2$  to generate the same high level representation on  $D_2$  as  $H_1$  does on  $D_1$  even though the style of the datasets is different. We do so by taking advantage of the content similarity between  $D_1$  and  $D_2$  which allows us to bypass the need for  $D_2$  annotations.

[1] addresses the issue of learning a “good representation” in the context of The Unsupervised and Transfer Learning Challenge. The test sets have examples which are not well represented in the training set. As a result, the input distribution of the training set is very different what appears in the test set and few or no labels are provided for some of the classes of interest. This is similar to the problem we address where  $D_2$  has a different distribution from  $D_1$  and there are no annotations for  $D_2$ . The solution they propose is to learn relevant representations for the non-annotated data using an unsupervised representation-learning algorithm. Their results are not as satisfying as they expect them to be and their explanation is that they lack annotated images. They argue that some of the relevant features should be learned on other instances than the non-annotated ones. So they use the annotated training set to build a set of relevant features for the training set and select the one that were also relevant for the non-annotated test set. We follow their guidelines as we first learn relevant semantic representations of the image content during the supervised training of  $D_1$ . Then we use these representations as a baseline to learn the relevant representations for  $D_2$ . Their work provide guidelines to unsupervised representation learning and experiments on classification dataset.

We extend their work to semantic segmentation for tasks where similar content representation naturally arises across distinct input distributions. This solves the challenge of the lack of annotated examples.

## 3 Method

### 3.1 Training

Figure 1 illustrates the training pipeline: the upper network has been trained in a supervised manner on an annotated dataset  $D_1$ . It has learned relevant high-level semantic representations of the image content and is then frozen (grey). The bottom network is initialised with the weights of the upper one and is trained on the second dataset  $D_2$ .  $D_2$  has content similar to  $D_1$  but with a different distribution. Given two images  $(X_1, X_2) \in D_1 \times D_2$ , the blue layers are fine-tuned to generate the same representation on  $X_2$  as the upper network on  $X_1$ . The training is a regression between feature maps and does not require any annotation on  $D_2$ .

More formally, let  $H(\theta)$  be a network model parameterised by weights  $\theta$  and  $\mathcal{F}(\theta) = \{F^l(\theta), l \in L\}$  a set of feature maps of the network  $H(\theta)$ . For example in VGG-16,  $\mathcal{F}(\theta)$  could be the `conv1_1` or `conv2_2` layer. Let  $H_1 = H(\theta_1)$  and  $H_2 = H(\theta_2)$  be two instances of  $H$  trained on  $D_1$  and  $D_2$ , leading respectively to the weights  $\theta_1$  and  $\theta_2$ .  $H_1$  is trained with the pixel-wise cross-entropy loss.  $H_2$  first initialised with the weights  $\theta_1$  and then trained on the set of image pairs  $\{(X_1^i, X_2^i), i \in I\} \subset D_1 \times D_2$ . Each pair has a similar content but different pixel distributions. However,  $H_2$  is not trained using the cross-entropy loss, but it is trained so that its feature maps  $\mathcal{F}(\theta_2) = \{F_2^l, l \in L\}$  match the corresponding feature maps  $\mathcal{F}(\theta_1) = \{F_1^l, l \in L\}$  from  $H_1$ . Given a set of feature map  $\mathcal{F}$ , for one image pair, the training loss is:

$$\begin{aligned} \mathcal{L}(H_2) &= \sum_{l \in L} w_l \mathcal{L}(F_2^l) \\ &= \sum_{l \in L} w_l \|F_1^l - F_2^l\|^2 \end{aligned} \tag{1}$$

Each feature map  $F_2^l$  generates a loss weighted by  $w_l$ . During training, the loss from the  $l$ -th feature map is back-propagated only in the layers lower than  $l$ . In our implementation, the feature weights has been kept constant. Investigations over more complex weighing strategies have been left for future work.

### 3.2 Evaluation

Following the standard practice in segmentation problems, we evaluate our method with the segmentation performance of  $H_2$  on the test set of  $D_2$ . We use both the mean class accuracy (acc) and the mean Intersection Over Union (IOU). The performances of  $H_2$  are compared to three baselines. The baseline B0 measures the performance of  $H_1$  on  $D_2$ , i.e. how well  $H_1$  generalises to a dataset with the same content but a different pixel distribution. This also gives a quantitative measure of the transformation between two datasets. The transformation is small when the performances of  $H_1$  on  $D_1$  and  $D_2$  are equivalent. The baseline B1 measures the performance of  $H_2$  trained from scratch on  $D_2$  when pixel-wise annotations are provided. This ideal setting provides the performance the transfer learning

B	Training	Test
B0	$H_1$ on annotated $D_1$	$H_1$ on $D_2$
B1	$H_2$ on annotated $D_2$	$H_2$ on $D_2$
B2	$H_2$ initialised with $\theta_1$ , fine-tuned on annotated $D_2$	$H_2$ on $D_2$

Table 1: Baselines summary.

should aim at. The last baseline B2 measures the performance of  $H_2$  when it is initialised with  $\theta_1$  and then fine-tuned on  $D_2$  using standard cross-entropy loss with full annotations. This provides the performance of classic supervised fine-tuning our method should reach, even though it does not require explicit annotations. The baselines are summarised in Table 3.2.

### 3.3 Visualisation

Once  $H_2$  is trained, we propose to visualise the changes of representation space induced by the regression. In principle, this is achieved by feeding an image  $X_1 \in D_1$  to  $H_2$  which generates a set of features  $\mathcal{F}_2(X_1)$ . We then need to design an optimisation for an image  $X$  initialised with noise so that  $\mathcal{F}_2(X)$  matches  $\mathcal{F}_2(X_1)$ . At the end of the optimisation,  $X$  should display the same content as  $X_1$  with the style of  $D_2$ .

To generate these images, we adapt the feature map inversion method from [10] to integrate style transfer into the inversion. In addition, we adapt the style transfer method from [6], [11] to generate image content and style from only one network instead of two.

In practice, the content and style generation is performed as follows: we feed  $X$  to  $H_2$ , compute a content loss and a style loss between  $\mathcal{F}_2(X_1)$  and  $\mathcal{F}_2(X)$ . Then we use Stochastic Gradient Descent (SGD) on  $X$  so as to make the features extracted from  $X$  converge to those extracted from  $X_1$ .

The loss used in the optimisation is computed for each feature map  $F_2^l$ . We use the loss definitions and Gram matrix definition from [6]. The content loss is a simple  $\mathcal{L}_2$  loss between feature maps. The style loss is a normalised  $\mathcal{L}_2$  loss between the Gram matrix of the feature maps. This matrix is computed from a 2D representation of each  $F_2^l$ .

$$\begin{aligned} \mathcal{L}_{content}(l) &= \frac{1}{2} \|F_2^l(X_1) - F_2^l(X)\|^2 \\ \mathcal{L}_{style}(l) &\propto \|G(F_2^l(X_1)) - G(F_2^l(X))\|^2 \end{aligned} \quad (2)$$

## 4 Experiments

### 4.1 Dataset

To compute the quantitative baselines, we use the PASCAL VOC12 [6] with three synthetic transformations. It contains 20 categories to segment and classify from an additional background category. The original dataset contains 1464 train images, 1449 validation images and 1456 test images. [6] provides additional annotated images resulting in 10 582 training

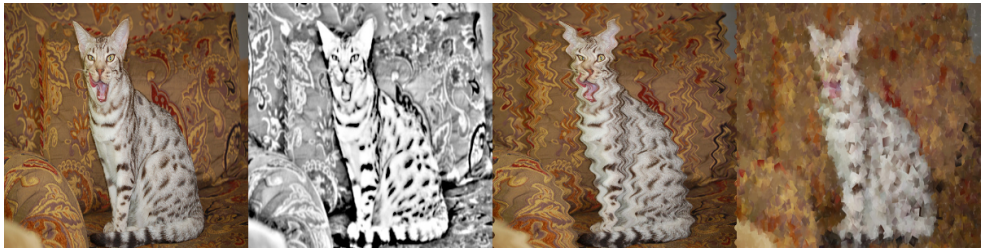


Figure 2: Synthetic transformations. Left-right: VOC, photocopy, ripple, cubism

T1: Photocopy	T2: Ripple	T3: Cubism
32.48	62.59	94.03

Table 2: Dataset distance and measure of the transformation complexity.

images. Three transformations are simulated on this dataset using GIMP<sup>1</sup> and illustrated in Figure 2. The regression is trained on the 10 582 original images together with their transformation.  $H_2$  is then evaluated on the transformed validation set resulting from each transformation.

$T_1$  is generated using the ‘photocopy’ filter which simulates a change of domain color with a change of saturation. This can be encountered in environment monitoring across long period of time such as land usage monitoring [15].  $T_2$  is generated with the ripple distortion to simulate misalignment of image content together with noise. This is typical in natural environment monitoring such as in the dataset from [6].  $T_3$  is generated with the cubism filter to simulate both a change of texture, misalignment with edge noise.

We measure the distance between the original PASCAL VOC 12 dataset  $D_1$  and a transformed dataset  $D_2$  (Table 2) with the normalized performance degradation of the network  $H_1$  between  $D_1$  and  $D_2$ . We train  $H_1$  on  $D_1$  following the setup from DeepLab V3 [8] and reach an accuracy of 79.92 and a mIOU of 69.22. Let  $acc_2$  and  $mIOU_2$  the performance of  $H_1$  on  $D_2$ , the distance is computed as follow:

$$d(D_1, D_2) = \frac{1}{2} \left( \frac{\|79.92 - acc_2\|}{79.92} + \frac{\|69.22 - mIOU_2\|}{69.22} \right) \quad (3)$$

From the normalized distances shown in Table 2, it is clear that the three transformation exhibit a increasing level of complexity that challenges a network trained only on  $D_1$ .

## 4.2 Experimental Setup

**Supervised training of  $H_1$ .**  $H$  follows the VGG-16 architecture [17] from DeepLabV3 [8] for training time considerations. The network reaches near state-of-the-art performance on PASCAL VOC 12 with only 5 hours of training on an NVIDIA Ge1080Ti. The training setting is the same as in [8]: we train the network for 20 000 iterations with a batch size of 10, stochastic gradient descent with a momentum of 0.9, a weight decay of 0.5 and the “poly” learning rate policy initialized at  $2.5 \times 10^{-4}$  with  $power = 0.9$ .

<sup>1</sup><https://www.gimp.org/>

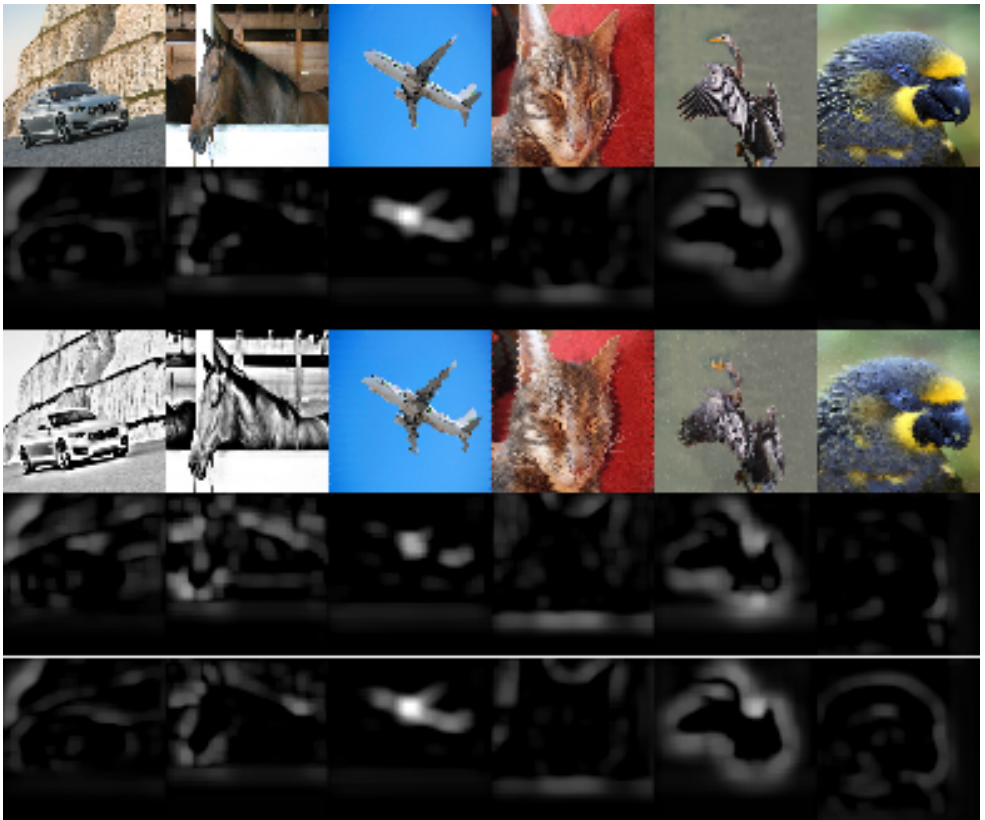


Figure 3: Feature map convergence. Line 1 show the original images. Line 2 show the feature map of  $H_1$  on  $D_1$ . Line 3 shows the transformed image. Line 4 show the feature map of  $H_1$  on  $D_2$ . Line 5 show the feature map of  $H_2$  on  $D_2$ .

**Feature map training of  $H_2$ .**  $H_2$  has the same architecture as  $H_1$ . We feed  $D_1$  to the trained  $H_1$ ,  $D_2$  to  $H_2(\theta)$  and train a regression between a set of feature map  $\mathcal{F}(\theta)$ . We chose several sets of feature maps to build  $\mathcal{F}$  to better understand the hierarchical representation model of the network. An intuition gathered from the literature ([1], [2], [3]) suggests that early layers captures low-level representations such as colors and edges, and deeper-level more complex representations such as object contours and their label. We evaluate this intuition by comparing the performance of  $H_2$  with regression on early layers such as `pool_1` or `pool_2` versus deeper layers such as `pool_5`. We also evaluate the correlation between these feature maps with regression on several layers simultaneously: `pool_1` to `pool_5`. Finally, we evaluate the relative importance of the features maps with two weights strategies. In the first one,  $w_l$  increases with the layer level, i.e.  $w_l$  is higher for `pool_5` than for `pool_1`. In the second, the weights are reversed. We use a uniform weight distribution [0.2, 0.4, 0.6, 0.8, 0.9].

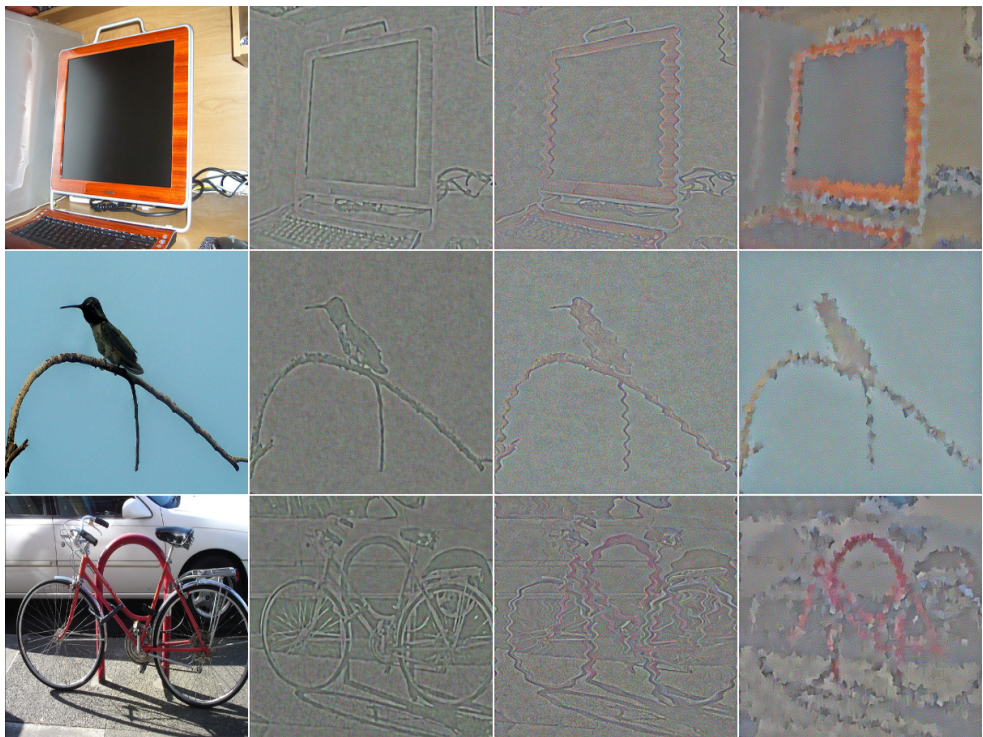


Figure 4: Style reconstruction:  $H_2$  is fed with the left-most image and generates a feature map. Then an image is generated to match this feature map. Left-right:  $H_2$  trained on  $T_1, T_2, T_3$ . The generated image match the content and the style transformation after 2000 iterations.

### 4.3 Experimental Results

Our method reaches comparable or better performance than fine-tuning on all transformation (Table 3). Let us recall however, that this is achieved without using an explicitly labeled segmentation on  $D_2$ . Figure 3 shows that the deep representations of  $H_2$  on  $D_2$  (bottom lines) converge towards the deep representation of  $H_1$  on  $D_1$  (Figure 3 line 2). Visualization (Figure 4) shows that this transfer learning method adapt the parameters to the dataset style. Reconstruction from the feature map shows the original image with the appropriate style.

B	T1	T2	T3
B0	54.73-46.07	31.76-24.28	5.18-3.78
B1	74.43-62.26	73.43-62.58	54.04-43.74
B2	<b>74.65</b> -63.41	74.71-63.99	<b>55.39</b> -45.37
Our	74.05- <b>64.39</b>	<b>78.65</b> - <b>67.23</b>	54.46- <b>45.79</b>

Table 3: Segmentation perf. of  $H_2$  on  $D_2$  for regression on pool\_5 (acc-mIOU)

Table 3 shows that our method reaches performances similar to classic fine-tuning for all image transformations. The first line (B0) shows the performance of  $H_1$  on the trans-



T	T1	T2	T3
pool_1	60.77-50.40	24.13-16.47	5.32-3.77
pool_2	65.84-54.26	25.59-17.72	7.03-5.55
pool_3	57.14-46.47	25.56-17.70	4.76-3.45
pool_4	4.76-3.45	25.53-17.67	43.25-35-14
pool_5	<b>75.05-64.39</b>	<b>78.65-67.23</b>	<b>54.47-45.79</b>
$W_{inc}$	69.27-59.15	4.76-3.45	35.24-29.44
$W_{dec}$	71.80-61.71	4.76-0.03	4.76-3.45

Table 4: Segmentation perf. of  $H_2$  on  $D_2$  for regression on different feature maps

formed dataset.  $H_1$  is trained with supervision on the original dataset  $D_1$ . So these metrics show the generalization properties of  $H_1$  on the transformed dataset. It also reflects the level of transformation between the original dataset and the transformed ones. For example, the photocopy dataset distribution is closer to the original dataset than the cubism dataset distribution: the accuracy drops from 54.73 to 5.18. Our method presents an improvement over all B0 results which means that transferring deep representations is a relevant transfer learning method for semantic segmentation. The second and third lines are the baselines we compare our method to: baseline B1 shows the performance of the network if trained from scratch on  $D_2$  when pixel-wise annotations are provided. Baseline B2 shows the performance of  $H_2$  when it is finetuned from  $H(\theta_1)$  with annotations of  $D_2$ . B2 outperforms B1 which confirms that transfer learning is relevant to DCNN even when pixel-wise annotations are provided. The third line shows our method always outperforms B2 with respect to mIOU and either outperform or reach comparable mean accuracy as B2. This shows that transfer learning of deep representations can replace classic DCNN finetuning.

Table 4 shows the segmentation performance of  $H_2$  when trained with different regression setting. The best performances are reached when the transfer learning is supervised between only the layers pool\_5 of each network. This suggests that the high level representation are the most relevant learning to transfer for semantic segmentation. The feature maps relevant to transfer may change with the nature of the transformation. The experiments do not provide a generic rule on the choice of the feature maps to transfer. But we can still draw an intuition with the results in Table 4. For  $T_1$ , we observe that transferring layers up to pool\_3 trains  $H_2$  to improve compared to B0 which is not the case for  $T_2$  and  $T_3$ . One explanation can be that  $T_1$  is only a texture transformation which conserves the alignment of the image. So the only change in the dataset is with regard to low-level features usually generated in early layers. However, in  $T_2$  and  $T_3$ , the contours of the semantic units in the images change. In  $T_2$  it is a regular change defined by the ripple parameters and for  $T_3$  the contour pattern is random. Object contours are features usually generated in deeper layers which can explain why the transfer of pool\_5 only is relevant for these datasets. The results also suggest that when low-level layers are not relevant to transfer, they can hinder the transfer of the relevant layers. For example, the transfer learning on multiple layers performs worse than the transfer on pool\_5 only. For  $T_3$ , we observe that a weight distribution that favors high layers performs better than  $W_{dec}$  but worse than the transfer of pool\_5. Future work will focus on the influence of the choice of the features maps in the transfer learning performance together with the choice of weight distribution.

## 5 Conclusion

This work extends the transfer learning of deep representations initiated in [10] to semantic segmentation. The application to recurrent dataset overcomes one of its limitation which is the lack of instance pairs with similar deep representations. For these applications, such pairs arise naturally. This method shows similar performance to classic fine-tuning without using annotations on the target task. The preliminary results suggest that the transfer learning is the most relevant between high layers. While this proof-of-concept targets the feasibility of this method, the experiments are not extensive enough to draw a relation between the transfer learning performance and the level of transferred deep representations. In future work, we will explore this dependence together with the correlation of transfer learning on multiple deep representations simultaneously.

## References

- [1] Vijay Badrinarayanan, Alex Kendall, and Roberto Cipolla. Segnet: A deep convolutional encoder-decoder architecture for image segmentation. *IEEE transactions on pattern analysis and machine intelligence*, 39(12):2481–2495, 2017.
- [2] Yoshua Bengio. Deep learning of representations for unsupervised and transfer learning. In *Proceedings of ICML Workshop on Unsupervised and Transfer Learning*, pages 17–36, 2012.
- [3] Liang-Chieh Chen, George Papandreou, Iasonas Kokkinos, Kevin Murphy, and Alan L Yuille. Deeplab: Semantic image segmentation with deep convolutional nets, atrous convolution, and fully connected crfs. *IEEE transactions on pattern analysis and machine intelligence*, 40(4):834–848, 2018.
- [4] Alexey Dosovitskiy and Thomas Brox. Inverting visual representations with convolutional networks. In *Proceedings of the IEEE Conference on Computer Vision and Pattern Recognition*, pages 4829–4837, 2016.
- [5] Mark Everingham, SM Ali Eslami, Luc Van Gool, Christopher KI Williams, John Winn, and Andrew Zisserman. The pascal visual object classes challenge: A retrospective. *International journal of computer vision*, 111(1):98–136, 2015.
- [6] Leon A Gatys, Alexander S Ecker, and Matthias Bethge. Image style transfer using convolutional neural networks. In *Computer Vision and Pattern Recognition (CVPR), 2016 IEEE Conference on*, pages 2414–2423. IEEE, 2016.
- [7] Shane Griffith, Georges Chahine, and Cédric Pradalier. Symphony lake dataset. *The International Journal of Robotics Research*, 36(11):1151–1158, 2017.
- [8] Bharath Hariharan, Pablo Arbeláez, Lubomir Bourdev, Subhransu Maji, and Jitendra Malik. Semantic contours from inverse detectors. In *Computer Vision (ICCV), 2011 IEEE International Conference on*, pages 991–998. IEEE, 2011.
- [9] Eddy Ilg, Nikolaus Mayer, Tomoy Saikia, Margret Keuper, Alexey Dosovitskiy, and Thomas Brox. Flownet 2.0: Evolution of optical flow estimation with deep networks. In *IEEE Conference on Computer Vision and Pattern Recognition (CVPR)*, volume 2, 2017.

- [10] Justin Johnson, Alexandre Alahi, and Li Fei-Fei. Perceptual losses for real-time style transfer and super-resolution. In *European Conference on Computer Vision*, pages 694–711. Springer, 2016.
- [11] Jonathan Long, Evan Shelhamer, and Trevor Darrell. Fully convolutional networks for semantic segmentation. In *Proceedings of the IEEE conference on computer vision and pattern recognition*, pages 3431–3440, 2015.
- [12] Aravindh Mahendran and Andrea Vedaldi. Understanding deep image representations by inverting them. In *The IEEE Conference on Computer Vision and Pattern Recognition (CVPR)*, June 2015.
- [13] Maxime Oquab, Leon Bottou, Ivan Laptev, and Josef Sivic. Learning and transferring mid-level image representations using convolutional neural networks. In *Computer Vision and Pattern Recognition (CVPR), 2014 IEEE Conference on*, pages 1717–1724. IEEE, 2014.
- [14] Sinno Jialin Pan and Qiang Yang. A survey on transfer learning. *IEEE Transactions on knowledge and data engineering*, 22(10):1345–1359, 2010.
- [15] Pradalier Cédric Perez Vincent Van Couwenberghe Rosalinde Durand Philippe Richard Antoine, Benbihi Assia. Automated segmentation and classification of land use from overhead imagery. In *Proceedings of the 14th International Conference on Precision Agriculture*, volume 2, 2018.
- [16] German Ros, Laura Sellart, Joanna Materzynska, David Vazquez, and Antonio M Lopez. The synthia dataset: A large collection of synthetic images for semantic segmentation of urban scenes. In *Proceedings of the IEEE Conference on Computer Vision and Pattern Recognition*, pages 3234–3243, 2016.
- [17] Karen Simonyan and Andrew Zisserman. Very deep convolutional networks for large-scale image recognition. *arXiv preprint arXiv:1409.1556*, 2014.
- [18] Karen Simonyan, Andrea Vedaldi, and Andrew Zisserman. Deep inside convolutional networks: Visualising image classification models and saliency maps. *arXiv preprint arXiv:1312.6034*, 2013.
- [19] Matthew D Zeiler and Rob Fergus. Visualizing and understanding convolutional networks. In *European conference on computer vision*, pages 818–833. Springer, 2014.